V International Scientific and Technical Conference Actual Issues of Power Supply Systems

Optimization of the technology for obtaining nanostructures based on AIIBVI compounds for photoenergetics

AIPCP25-CF-ICAIPSS2025-00567 | Article

Optimization of the technology for obtaining nanostructures based on $A^{II}B^{VI}$ compounds for photoenergetics

Khalmurat Iliev[1], Nurillo Zikrillaev[1], Usmonkhuja Sodikov[1, a)], Stanislav Tachilin[1], Abrorjon Gulomov[1], Abdurakhmon Khasanov[2]

[1] Tashkent State Technical University named after Islam Karimov, Tashkent, Uzbekistan
[2] Università degli Studi della Tuscia, Viterbo, Italy

[a] Corresponding author: sodikovusmonhoja@gmail.com

Abstract. This article addresses one of the fundamental challenges in modern power engineering the development of high-efficiency solar cells by analyzing and optimizing technological processes for obtaining nanostructures of $A^{II}B^{VI}$ group compounds (ZnS, CdS, ZnTe, CdTe, etc.) on silicon-based materials. The article examines the interaction features of $A^{II}B^{VI}$ nanocomposites with silicon, heterojunction formation, diffusion processes, and thermodynamic conditions for increasing the concentration of $A^{II}B^{VI}$ nanocomposites on the surface and in the bulk of silicon. It is shown that the correct selection of diffusion process conditions will significantly improve the morphology of nanostructures and integrate $A^{II}B^{VI}$ materials into silicon technology to create new materials, enabling the fabrication of fundamentally new solar cells capable of producing ultrahigh efficiency, low-cost solar cells for the solar power industry.

INTRODUCTION

Materials of groups II–VI introduced into the silicon lattice enable targeted modification of electronic states in local regions and the formation of zones of direct interband transitions, which is unattainable in pure silicon. Of particular interest are silicon-based ZnS, CdS, ZnTe, and CdTe nanostructures, since their energy levels and crystal-chemical characteristics have a strong impact on the local bonding configuration within the tetrahedral Si framework. Unlike traditional surface deposition techniques, diffusion-driven incorporation of these elements creates favorable conditions for forming binary nanoclusters (BNC) of $A^{II}B^{VI}$ compounds both at the surface and inside the silicon lattice. This fundamentally alters the optical and electronic parameters of the semiconductor material, making it a promising candidate for next-generation solar cells with ultrahigh efficiency and low cost.

The primary difficulty in obtaining BNC of $A^{II}B^{VI}$ in silicon stems not only from lattice mismatch (up to 15÷20% for several impurity pairs) but also from the differences in their preferred coordination states. For example, Zn and Se atoms in silicon tend to form localized complexes with distorted tetrahedral geometries, which, under improper processing conditions, may lead to defect-rich layers and instability of Si–Si bonds. One of the most effective approaches for improving heterostructure quality is the use of multi-stage temperature regimes during impurity introduction. The sequential alteration of thermodynamic conditions in such regimes helps reduce defect density, relax internal stresses, and promote the formation of a more ordered crystalline structure.

Integrating $A^{II}B^{VI}$ materials with monocrystalline silicon enables the development of hybrid heterostructures that combine the optoelectronic advantages of $A^{II}B^{VI}$ compounds with the technological compatibility of silicon. Nonetheless, significant disparities in lattice parameters, coefficients of thermal expansion, and chemical reactivity create substantial challenges for producing high-quality nanostructures. From a technological standpoint, it is crucial to control not only the temperature but also its rate of change to ensure that the process promotes clustering of incorporated impurities rather than the destruction of surface bonds [1–10].

The objective of this work is to justify and optimize the technological processes for synthesizing $A^{II}B^{VI}$ nanostructures within monocrystalline silicon and to identify the factors that govern their interactions within the silicon lattice. When forming $A^{II}B^{VI}$ nanostructures inside silicon, several key issues that affect the defectiveness of the main material must be taken into account. First, the mismatch in lattice parameters, i.e., differences in lattice

periods may reach 15÷20%, leading to increased stresses and defect formation at the interface. Second, $A^{II}B^{VI}$ structures possess higher coefficients of thermal expansion, resulting in thermal mismatch during post-diffusion cooling and the development of internal stresses that affect nanostructure morphology. Third, the silicon surface is prone to oxidation, which leads to the formation of an amorphous SiO_2 layer that inhibits the growth and concentration of nanostructures at both the surface and within the bulk. Therefore, optimization of impurity introduction via diffusion techniques must consider controlled surface preparation, accurate management of growth parameters, and prevention of defect-layer formation.

EXPERIMENTAL RESEARCH

One of the methods used to obtain such structures is chemical vapor deposition. CVD and MOCVD techniques are widely applied for the growth of ZnO nanorods and CdS and CdSe thin films. These methods ensure high material purity and precise thickness control. Their advantages include uniform deposition, high growth rates, and the possibility of epitaxial growth on silicon substrates. However, the need for strict temperature control and the complexity of the equipment limit their applicability for producing silicon samples with $A^{II}B^{VI}$ based structures.

The molecular beam epitaxy (MBE) method is also extensively used to obtain high-quality CdTe/Si and ZnSe/Si heterostructures. Its key advantages include atomically precise control of source fluxes, the capability of growth at relatively low temperatures, and the formation of layers with a minimal concentration of structural defects.

Chemical bath deposition (CBD) is among the most accessible and widely used techniques for obtaining CdS, ZnS, CdSe, and ZnSe nanocrystals. This approach is distinguished by its low processing temperature, technological simplicity, and the ability to form quantum dots. At the same time, it has a significant drawback namely, the comparatively low crystalline quality of the resulting material.

Electrochemical deposition is mainly employed to form ordered arrays of ZnO and CdTe nanorods. This method provides precise control over structural morphology and uniform distribution across the substrate. The pulsed laser deposition (PLD) technique allows effective control of nanostructure growth parameters, including size, shape, and chemical composition. However, these technologies require sophisticated and expensive equipment, which limits their use in large-scale production.

Preparation of the silicon substrate plays a crucial role in the successful growth of $A^{II}B^{VI}$ compound nanostructures. One of the initial steps is the removal of the native oxide layer, which can be achieved through HF chemical etching, plasma cleaning, or vacuum desorption at 700–800 °C. To improve adhesion and reduce mechanical stress, surface nanostructuring of silicon such as formation of a microporous layer is often employed. Additionally, the use of buffer layers, such as ZnS, ZnSe, CdS, and CdSe, is an important technological measure. These layers reduce lattice mismatch and provide more stable conditions for the growth of $A^{II}B^{VI}$ nanostructures.

Optimization of growth parameters has a decisive influence on the morphology and physical properties of the resulting semiconductor materials. Deposition temperature determines crystallite size, defect concentration, and growth mode (two-dimensional or three-dimensional). Increased temperature typically leads to grain enlargement; however, excessively high temperature may trigger diffusion processes and disrupt stoichiometry. The partial pressures of the components during $A^{II}B^{VI}$ synthesis are also essential, as deviations from stoichiometric balance can lead to an excess of the chalcogenide component, vacancy formation, and reduced optical transparency. Growth rate is another critical parameter: if it is too high, porous and loose structures may form, whereas an excessively low growth rate promotes crystallite enlargement and higher dislocation density. Additional control over the morphology of ZnS nanorods is achieved by using catalytic layers (Au, Ag, or Cu), which determine growth orientation and promote the formation of homogeneous nanocolumns.

The morphological features of $A^{II}B^{VI}$ nanostructures on silicon substrates are studied using scanning electron microscopy (SEM) and atomic force microscopy (AFM), which allow assessment of surface uniformity, nanostructure size, and their spatial distribution.

The crystalline quality of the samples is evaluated using X-ray diffraction (XRD), which provides information on the parallelism of crystal planes, the level of internal lattice stress, and the presence of structural defects. The optical properties of the nanostructures are analyzed based on photoluminescence (PL) measurements and optical absorption spectra (UV–Vis). High-quality $A^{II}B^{VI}$ nanostructures are characterized by narrow photoluminescence peaks and spectral shifts into the quantum-confinement region, indicating a low defect density and well-controlled nanocrystal size.

One of the effective approaches to synthesizing BNC of $A^{II}B^{VI}$ is the use of multistage temperature regimes during diffusion processes, which enable significant increases in impurity penetration depth, concentration, and

reduced structural defect formation. Growth of nanostructures is facilitated by optimized thermodynamic conditions, impurity vapor pressures, and pre-modified silicon surfaces, contributing to the formation of horizontally oriented nanorod arrays. Additional laser or thermal treatment enhances clustering processes both within the bulk and on the silicon surface, increases photoluminescence intensity, and improves crystallinity. Thus, integrating $A^{II}B^{VI}$ nanostructures with silicon photonics is considered a promising direction for creating high-efficiency solar cells and photovoltaic devices with ultrahigh efficiency and reduced manufacturing cost.

RESEARCH RESULTS

Industrial single-crystal silicon samples of grades KEF-4.5 and KDB-0.1, 0.5, and 1 were selected as the initial materials for this study. Their phosphorus concentrations were in the range of $N_P=9,3*10^{14}$ sm^{-3} and boron concentrations were $N_B=2,1\times10^{17}$; $4,2\times10^{16}$ and $2,1\times10^{16}$ sm^{-3} respectively. Elements from groups II and VI were used as diffusing impurities. Fundamental electrical parameters of the obtained samples were measured using single-probe and four probe methods, while additional characteristics were determined using the modernized IRS-12 system, FSM-1202, and the INFRAM-I infrared microscope. Digital instruments UT81, Mastech MS8250D, and DT-9205 were employed for photoelectric measurements. The structural state of BNC of $A^{II}B^{VI}$ within the silicon lattice was examined using a SEM EVO MA10 (Carl Zeiss) scanning electron microscope, an Aztec Energy Advanced X-act (Oxford Instruments) X-ray microanalysis system, and powder X-ray diffractometers XRD Empyrean (PAnalytical).

A specialized diffusion doping technology with multi-stage slow temperature elevation was developed for this research. This approach provides uniform doping of silicon while preventing surface erosion. Under doping temperatures of 1150÷1250 ^{0}C for 30÷180 minutes, no signs of surface degradation were observed in samples processed with group II and VI impurities inside quartz ampoules evacuated to 10^{-5} mmHg. The resulting material containing $A^{II}B^{VI}$ type of BNC structures demonstrated a broadened spectral response of silicon photodetectors, particularly in the infrared region. Thus, the diffusion-based formation of $A^{II}B^{VI}$ nanostructures in the silicon lattice significantly expands the operational sensitivity of silicon based IR devices.

For the obtained samples, optimal diffusion parameters were established that ensure uniform incorporation of BNC structures with the required concentration, together with controlled spatial distribution and ordering. The BNC enriched layer reached several tens of micrometers in thickness, which is sufficient for structural, electrical, and spectral analysis. Figure 1 illustrates the model of $Si_2A^{II}B^{VI}$ of BNC formation within the monocrystalline silicon lattice.

To perform comprehensive studies, a diffusion-doping technique based on multi-stage and quasi-isothermal temperature elevation was developed. This heating scheme ensures a homogeneous doping profile throughout the silicon crystal while eliminating the risk of surface erosion or thermally induced structural defects. Experiments conducted at 1150÷1250 °C for 30÷180 minutes under deep vacuum conditions (approximately 10^{-5} mmHg) inside sealed quartz ampoules confirmed that no surface degradation, roughening, or matting occurred during the incorporation of group II and VI elements, demonstrating the stability of the silicon surface under these conditions.

The material obtained after diffusion of impurity atoms exhibited the formation of binary nanoclusters of the $A^{II}B^{VI}$ type embedded within the silicon lattice. These clusters fundamentally modify both local and bulk electronic properties of the semiconductor. It was established that the presence of such impurity complexes leads to a broadening of the spectral sensitivity range of silicon-based photoconverters, especially in the infrared region. This enhancement can be attributed to modifications in the density of electronic states, local distortions of the crystal field, and the emergence of additional allowed energy levels that influence interband transitions. Therefore, the developed cluster of $A^{II}B^{VI}$ incorporation technology serves as an effective method for improving the sensitivity of silicon IR detectors and other optoelectronic systems.

For the fabricated samples, optimal kinetic and thermodynamic diffusion parameters were identified, ensuring uniform spatial distribution of BNC structures with the desired concentration and controlled degrees of ordering. It was confirmed that the BNC enriched layer, with a thickness of several tens of micrometers, is adequate for subsequent structural, spectroscopic, and electrical characterization. Figure 1 presents a model schematic illustrating the formation of $Si_2A^{II}B^{VI}$ structures within the monocrystalline silicon lattice, including the coordination environment of impurity atoms and the configuration of the local tetrahedral sublattice.
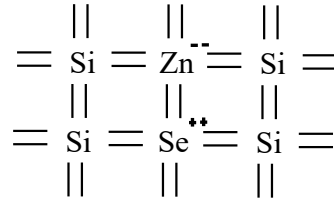
$$
\begin{array}{ccccc}
\| & & \| & & \| \\
= \mathrm{Si} = & \mathrm{Zn} = & \mathrm{Si} = \\
\| & & \| & & \| \\
= \mathrm{Si} = & \mathrm{Se} = & \mathrm{Si} = \\
\| & & \| & & \|
\end{array}
$$

FIGURE 1. Formation of the BNC with the $\mathrm{Si_2A^{II}B^{VI}}$ structure in the lattice of monocrystalline silicon.

The formation of rational impurity-atom pairs from group II and group VI elements for incorporation into the crystalline structure of silicon was carried out based on an extended set of structural–electronic criteria aimed at achieving maximal thermodynamic and configurational compatibility with the tetrahedral Si sublattice. One of the key requirements was that the total number of valence electrons of two adjacent impurity atoms approach eight, since such electronic saturation minimizes perturbation of the local hybridization and supports preservation of the characteristic sp³ coordination inherent to the silicon lattice.

An equally important parameter is the correspondence between the electronegativity of the introduced atoms and that of silicon. The energetic magnitude of electron-density redistribution during heterocoordination substitution is governed by the degree of bond polarization and the relative electron-acceptor capacity of the impurity center. When electronegativities differ significantly, the probability of forming metastable configurations, local defects, and an increase in the system's free energy becomes higher.

The kinetic geometric criterion included the requirement is $r_m \leq 100R$, where r_m is the interatomic distance between the considered particles both in the initial and post-diffusion states, and R=5.4 A° is the lattice constant of silicon. This constraint reflects the necessity of minimizing the deformation potential and preventing the emergence of excessive local stresses that could impede the formation of stable binary nanoclusters.

Additionally, the deviation of the covalent radii of the impurity atoms from that of silicon was analyzed according to the relation:

$$|\Delta Z| = 2Z_{Si} - \left(Z_{(II)} + Z_{(VI)}\right) \leq 0{,}2\,Z_{Si}, \tag{1}$$

where Z_{Si} — is the covalent radius of the silicon atom, and $Z_{(II)}\ and\ Z_{(VI)}$ are the covalent radii of the group II and group VI impurity atoms, respectively. Compliance with this condition ensures minimization of geometric distortions in the coordination sphere, including preventing rupture or excessive deformation of tetrahedral bonds, which ultimately increases the probability of forming energetically stable binary impurity complexes.
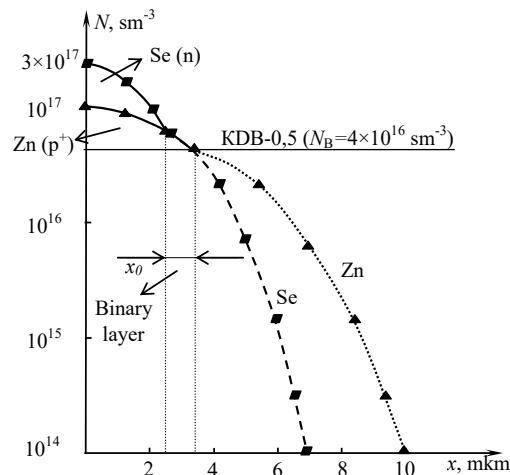

FIGURE 2. Formation of a BNC with the $\mathrm{Si_2ZnSe}$ structure in the near-surface region of the monocrystalline silicon lattice.

Simultaneous fulfillment of these criteria makes it possible not only to predict feasible configurations of impurity pairs within the silicon lattice, but also to establish a foundation for further modeling of energy profiles, diffusion barriers, and the stability of the resulting nanostructures over a broad range of thermodynamic parameters. Figure 2 shows the mechanism of BNC formation involving impurity atoms Zn and Se from group II and group VI, respectively.

The low-temperature method for forming binary nanostructures (BNC) of the Si_2ZnSe type in the near-surface region of monocrystalline silicon involves a multi-stage thermomigrational treatment of the material, with a gradual and strictly controlled increase in temperature. The sequence of operations was designed to ensure both phase and configurational stability of the forming clusters while minimizing the probability of defects associated with distortion of the tetrahedral Si sublattice.

At the initial stage, selenium was selected as the first impurity because of its high chemical compatibility with the silicon matrix. The diffusion parameters of Se were calculated using classical exponential relations:

$$D_{Se} = 9 \times 10^{-1} \times \exp\left(\frac{-2,44}{kT}\right) \tag{2}$$

$$N_{Se} = 1,4 \times 10^{25} \times \exp\left(\frac{-2,3}{kT}\right) \tag{3}$$

where D_{Se} is the diffusion coefficient of selenium, N_{Se} is the equilibrium solubility of selenium in Si, k is the Boltzmann constant, and T is the absolute temperature of the process.

Prepared quartz ampoules, evacuated to approximately 10^{-5} mmHg and containing the silicon samples, were placed into the working zone of a horizontal furnace at room temperature. Thermal treatment was carried out at 1200÷1250 °C for 30÷60 minutes, after which the ampoules were slowly cooled on a metallic heat sink. This regime prevented the formation of temperature gradients and preserved the integrity of the sample surfaces.

At the next stage, zinc an element of group II necessary for forming $A^{II}B^{VI}$ type nanostructures was introduced as the second impurity. Its diffusion characteristics are described by the relations:

$$D_{Zn} = 1 \times 10^{-1} \times \exp\left(\frac{-1,5}{kT}\right) \tag{4}$$

$$N_{Zn} = 4,0 \times 10^{21} \times \exp\left(\frac{-1,6}{kT}\right) \tag{5}$$

where D_{Zn} is the diffusion coefficient of zinc and N_{Zn} is its equilibrium solubility in Si, k is the Boltzmann constant, and T is the absolute temperature of the process.

A quartz ampoule containing the pre-doped Si<B,Se> samples together with the zinc source was then placed into the furnace at room temperature. The diffusion process proceeded at 1200÷1250 °C for 2 hours. After completing diffusion, the ampoules were cooled in the same slow, controlled manner on metal, preventing thermomechanical damage.

It should be emphasized that control experiments based on classical diffusion procedures for group II and VI elements were carried out in parallel. These experiments allowed comparison of the obtained parameters with traditionally doped samples and clearly demonstrated the advantages of the proposed cluster-formation technology.

The final stage of the process aimed to increase both the concentration and the degree of ordering of the formed binary nanostructures. The processed samples underwent prolonged annealing at reduced temperatures of 500÷800 °C for 4÷6 hours. The choice of a low-temperature regime is essential, as it provides energetically favorable conditions for the coordinated approach of doubly positively charged ions of group II elements and doubly negatively charged Se ions. Their arrangement in neighboring lattice sites promotes the self-assembly of Si_2ZnSe nanoclusters (Fig. 3), accompanied by an expansion of the BNC enriched layer - both in depth and in concentration.

As follows from the impurity-concentration distribution profile (Fig. 3), the enriched Zone of BNC tends to increase in thickness, confirming the effectiveness of the sequential three stage thermodiffusion treatment and demonstrating the significant impact of the process on the optical and electrical properties of the modified silicon.
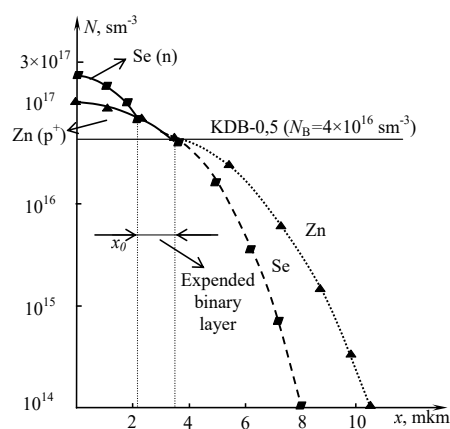
FIGURE 3. Additional annealing of Si$_2$<BZnSe> samples at T = 400 °C, t = 4 hours.

Figure 4 presents a model of the spatial arrangement of a BNC with the Si$_2$ZnSe structure in the silicon lattice. As seen from this model, the newly formed material constitutes an entirely new type of compound characterized by a strong partially ionic-covalent bond, distinct from either purely covalent or purely ionic bonding. Such a hybrid bonding configuration reflects the unique electronic interaction between Zn and Se within the tetrahedral coordination environment of silicon.
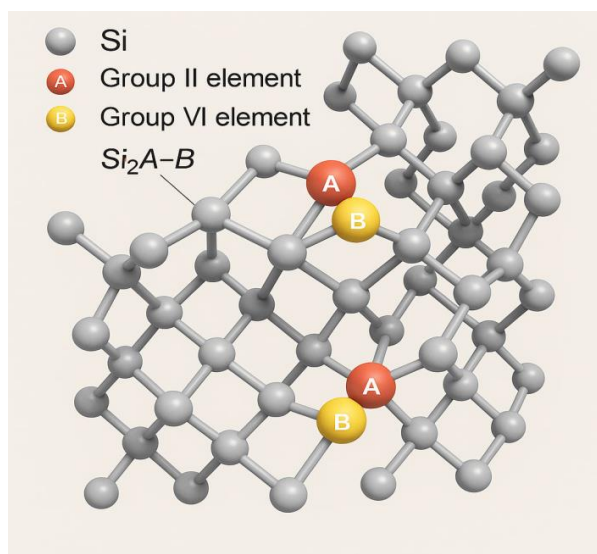

FIGURE 4. Model of a BNC with the Si$_2$Zn$^-$Se^{++} (Si$_2$A^{II}B^{VI}) structure in the silicon lattice.

$$
\begin{array}{ccccccccccccccc}
\| & & \| & & \| & & \| & & \| & & \| & & \| & & \| \\
= & \text{Si} & = & \text{Si} & = & \text{Si} & = & \text{Si} & = & \text{Si} & = & \text{Si} & = & \text{Si} & = & \text{Si} & = \\
\| & & \| & & \| & & \| & & \| & & \| & & \| & & \| \\
= & \text{Si} & = & \text{Se}^{++} & = & \text{Zn} & = & \text{Se}^{++} & = & \text{Zn} & = & \text{Se}^{++} & = & \text{Zn} & = & \text{Si} & = \\
\| & & \| & & \| & & \| & & \| & & \| & & \| & & \| \\
= & \text{Si} & = & \text{Zn} & = & \text{Se}^{++} & = & \text{Zn} & = & \text{Se}^{++} & = & \text{Zn} & = & \text{Se}^{++} & = & \text{Si} & = \\
\| & & \| & & \| & & \| & & \| & & \| & & \| & & \| \\
= & \text{Si} & = & \text{Si} & = & \text{Si} & = & \text{Si} & = & \text{Si} & = & \text{Si} & = & \text{Si} & = & \text{Si} & = \\
\| & & \| & & \| & & \| & & \| & & \| & & \| & & \|
\end{array}
$$

FIGURE 5. Arrangement of BNC nanoclusters with the Zn^-Se^{++} ($A^{II}B^{VI}$) structure in the silicon lattice.

An increase in the concentration of $A^{II}B^{VI}$ type structures (up to 10^{16} sm^{-3}) enables the formation of BNC of the Zn^-Se^{++} type (Fig. 5). This represents an entirely new material whose properties differ fundamentally from those of the original constituents, resulting in qualitatively different processes within the crystal. As a consequence, regions with locally direct bandgap behavior emerge both on the surface and within the bulk of the material. Ultimately, parameters such as carrier mobility, carrier lifetime, and the optical absorption coefficient of the new material undergo significant modification.

This means that, based on a single silicon crystal lattice, by forming nanocrystals of various structures (Si, Si<B,Se>, Si<B,Zn>, and Si$_2$ZnSe) and Zn^-Se^{++} associations, it becomes possible to obtain a material with a deliberately engineered, modulated bandgap width.

Using the formation of BNC structures from group II and VI impurity atoms within the silicon lattice, new types of solar cells and photodetectors were developed, featuring expanded spectral sensitivity extending into the infrared (IR) and ultraviolet (UV) regions. A laboratory scale photovoltaic element based on $Si_2A^-B^{++}$ BNC structures was designed and fabricated. The fundamental parameters of this new photovoltaic device were investigated. Figure 6 shows a schematic design of the solar cell incorporating a BNC $Si_2A^{II}B^{VI}$ structure within the silicon matrix.

upper metal contact

$$ n^+ $$

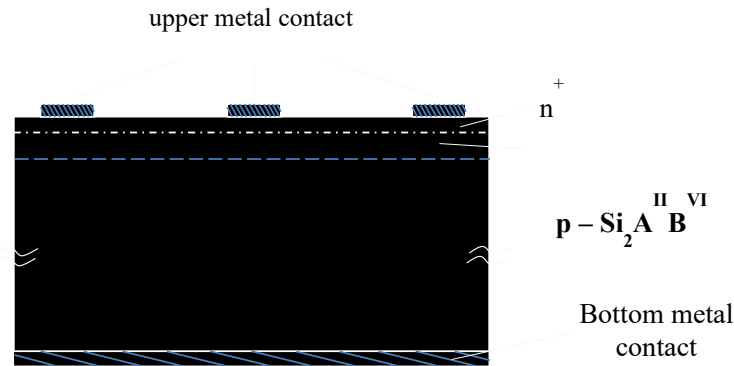$$ p - Si_2A^{II}B^{VI} $$

Bottom metal contact

FIGURE 6. Schematic design of the developed photovoltaic element with a $Si_2A^{II}B^{VI}$ BNC structure based on silicon.

Experimental comparison of the spectral response of photovoltaic elements containing Si_2ZnSe type BNC fabricated using the low-temperature synthesis method with conventional photovoltaic elements produced by standard technology demonstrated a significant broadening of the spectral sensitivity range. The BNC based devices manufactured using the new method exhibited a spectral sensitivity coefficient 2.5 times higher than that of the cells produced by conventional technology. The results of the light I–V characteristic analysis for Si_2ZnSe based BNC photovoltaic elements fabricated by the new method, using infrared (IR) filters, are presented in Table 1.

TABLE 1. $(\frac{I_{cc_1.}}{I_{cc_2.}})$ and $(\frac{U_{oc_1.}}{U_{oc_2.}})$- percentage values for BNC based and conventional photovoltaic elements under identical conditions. $I_{cc_1.}$, $U_{oc_1.}$ - measurements performed with an IR filter and $I_{cc_2.}$, $U_{oc_2.}$ - measurements obtained without filtering.

Sample	I	II	III	IV	V	Traditional solar cells
$\dfrac{I_{cc_1.}}{I_{cc_2.}}$	68%	27%	44%	41%	21%	4,7%
$\dfrac{U_{oc_1.}}{U_{oc_2.}}$	76%	70%	54%	49%	46%	42%

As can be seen from Table 1, while commercial silicon-based photovoltaic elements exhibit a value of $\frac{I_{cc_1.}}{I_{cc_2.}}$=4.7%, in our BNC based photovoltaic elements this value reaches 68%, which is roughly 15 times higher. For industrial samples, the ratio $\frac{U_{oc_1.}}{U_{oc_2.}}$ is 42%, whereas in the photovoltaic elements developed in this work it reaches 70%.

The emergence of these enhanced properties during the formation BNC of $Si_2A^{II}B^{VI}$ type clusters are associated with a redistribution of the electronic energy structure in localized regions due to increased impurity concentration and controlled spatial arrangement of these impurity atoms within the silicon lattice. This enables the use of the newly engineered materials to develop a fundamentally new class of highly efficient solar cells and solar modules with ultra-high performance and low manufacturing cost.

CONCLUSIONS

The integration BNC of $A^{II}B^{VI}$ nanostructures with elements of silicon photonics represents a strategically important direction in the development of modern optoelectronic technologies. Such integration opens the possibility of designing high-efficiency photovoltaic converters for solar energy applications, as well as highly sensitive infrared photodetectors intended for next-generation sensing systems.

Optimization of the technological processes used to obtain $A^{II}B^{VI}$ nanostructures in silicon is a key stage in the advancement of hybrid optoelectronics. Proper silicon surface preparation, precise control over growth parameters, the use of buffer layers, and appropriate structural diagnostics collectively enable substantial improvements in material quality. Further research in this field holds promise for the creation of new solar batteries with ultra-high efficiency and low production cost, significantly expanding the potential of silicon-based solar energy technology.

REFERENCES

1. Jungwirth T., Sinova J., Masek J., Kucera J., MacDonald A.H. Theory of ferromagnetic (III, Mn) V semiconductors. Reviews of Modern Physics, 2006, 78(3), pp. 809–864. https://doi.org/10.1103/RevModPhys.78.809
2. Bonanni A., Dietl T. A story of high-temperature ferromagnetism in semiconductors. *Chem. Soc. Rev.*, 2010, 39(2), pp. 528–539. https://doi.org/10.1039/B909298
3. Utamuradova, Sh. B., Mavlyanov, A. Sh., Sobirova, Sh. A., Sattarov O.E., Hybrid Secondary Structure of Manganese and Sulfur in Silicon, *Surface Engineering and Applied Electrochemistry,* 2025, Vol.61, p. 633. . https://doi.org/10.3103/S1068375525700681
4. Hakkulov M.K, Mavlyanov A.Sh., Sattarov O.E., Akbarova N.A., Kamalova Kh.K., Formation of Binary Compounds of Impurity Atoms of Sulfur and Zinc in Silicon, Surface Engineering and Applied Electrochemistry, 2024, Vol. 60, p. 826. . https://doi.org/10.3103/S106837552470042
5. Bakhadyrkhanov, M.K., Iliev, K.M., Mavlonov, G.K., Ibodullaev, S.N., Tachilin, S.A., The Effect of Negative Magnetoresistance in Silicon to Create Multifunctional Sensors, Technical Physics Letters, 2022, 48(1), p. 1. . https://doi.org/10.1134/S1063785022010023
6. Bakhadyrhanov M. K., Sodikov U. X., Melibayev D., Tuerdi Wumaier, Koveshnikov S. V., Khodjanepesov K. A., Jiangxiang Zhan Silicon with Clusters of Impurity Atoms as a Novel Material for Optoelectronics and

Photovoltaic Energetics. Journal of Materials Science and Chemical Engineering, USA. Apr. 30, 2018, 6, 180-190. . https://doi.org/10.4236/msce.2018.64017

7. Bakhadyrhanov M.K., Sodikov U.X., Iliev Kh.M., Tachilin S.A., Tuerdi Wumaier Perspective Material for Photoenergetics on the Basis of Silicon with Binary Elementary Cells. USA. Journal of Materials Physics and Chemistry, 2018, Volume 1, pp. 1-7. (RG (40), https://doi.org/10.63019/mpc.v1i2.493

8. Bakhadyrkhanov M.K., Mavlyanov A.Sh., Sodikov U.Kh., and Khakkulov M.K., "Silicon with Binary Elementary Cells as a Novel Class of Materials for Future Photoenergetics", Applied Solar Energy, 51(4), 258–261 (2015). https://doi.org/10.3103/S0003701X1504009X

9. Liu J., Yue S., "Fabrication of ZnS layer on silicon nanopillars surface for photoresistor application," Chemical Physics Letters, 801, 139716 (2022). https://doi.org/10.1016/j.cplett.2022.139716

10. Kang J., Park J.-S., Stradins P., and Wei S.-H., "Nonisovalent Si-III-V and Si-II-VI alloys: Covalent, ionic, and mixed phases," Physical Review B, 96, 045203 (2017). https://doi.org/10.1103/PhysRevB.96.045203

11. Zikrillaev N.F., Khakkulov M.K., and Isakov B.O., "The mechanism of the formation of binary compounds between Zn and S impurity atoms in Si crystal lattice," East Eur. J. Phys. (4), 177 (2023). https://doi.org/10.26565/2312-4334-2023-4-20

12. Abdurakhmanov B. A., Bakhadirkhanov M. K., Iliyev H. M., Isamov S. B., Saitov E. B., Mavlyanov A., Kamalov H. U., Saparniyazova Z., Sattarov O., Sodikov U. Kh., Zikrillayev N. F. Silicon with Clusters of Impurity Atoms as a Novel Material for Photovoltaics. USA, Nanoscience and Nanotechnology 2014, 4(3): pp. 41-43. © Index Copernicus 2014 https://doi.org/10.5923/j.nn.20140403.01

13. Bakhadyrkhanov, M.K., Mavlonov, G.K., Isamov, S.B., Tachilin, S.A., Photoconductivity of silicon with multicharged clusters of manganese atoms [Mn]4, Surface Engineering and Applied Electrochemistry, 2010, 46(3), p. 276. . https://doi.org/10.3103/S1068375510030154

14. Bakhadyrkhanov, M.K., Ayupov, K.S., Iliev, K.M., Mavlonov, G.K., Tachilin, S.A., Effect of electric field, illumination, and temperature on negative magnetoresistance of low-temperature-diffusion-doped silicon, Technical Physics Letters, 2010, 36(8), p. 741. . https://doi.org/10.1134/S1063785010080195

15. Bakhadirkhanov, M.K., Mavlonov, G.H., Iliev, X.M., Sattarov, O.E., Tachilin, S.A., Specific features of magnetoresistance in overcompensated manganese-doped silicon, Semiconductors, 2014, 48(8), p. 986. . https://doi.org/10.1134/S106378261408003

16. Kim S., Park J., Kim D., et al. Magnetic properties of Mn-doped Si nanostructures prepared by ion implantation and annealing. Journal of Applied Physics, 2019, 125(17), 173904. https://doi.org/10.1063/15085030

17. Dietl T., Ohno H., Matsukura F., Cibert J., Ferrand D. Zener model description of ferromagnetism in zinc-blende magnetic semiconductors. *Science*, 2000, 287(5455), p. 1019–1022. https://doi.org/10.1126/287.5455.1019

18. Bakhadirkhanov M.K., Zikrillaev N.F., Narkulov N., Sadykov U.Kh., Tuerdi Umaier and Ayupov K.S. The concentration of electroactive atoms of transition group elements in silicon USA, Surface Engineering and Applited Electrohemistry, USA, 2005, No.2, pp.90-93.

19. Zikrillayev N.F., Isamov S.B., Isakov B.O., Wumaier T., Liang Li wen, Zhan J.X., and Xiayimulati T., "New Technological Solution for the Tailoring of Multilayer Silicon-based Systems with Binary Nanoclusters Involving Elements of Groups III and V," Journal of nano- and electronic physics, 15(6), 06024 (2023). https://doi.org/10.21272/jnep.15(6).06024

20. Zikrillaev N.F., Kushiev G.A., Hamrokulov Sh.I., and Abduganiev Y.A., "Optical Properties of GexSi1-x binary compounds in silicon," Journal of nano- and electronic physics, 15(3), 03024-1 - 03024-4, (2023). https://doi.org/10.21272/jnep.15(3).03024

21. Zikrillaev N.F., Tursunov O. B., and Kushiev G. A., "Development and Creation of a New Class of Graded-Gap Structures Based on Silicon with the Participation of Zn and Se Atoms," Surf. Engin. Appl. Electrochem. 59(5), 670–673 (2023). https://doi.org/10.3103/S1068375523050198

22. Zikrillaev N.F., Koveshnikov S.V., Isamov S.B., Abdurahmonov B.A., and Kushiev G.A., "Spectral dependence of the photoconductivity of Ge_xSi_{1-x} type graded-gap structures obtained by diffusion technology," Semiconductors, 56(1), 29-31 (2022). https://doi.org/10.1134/S1063782622020191